Role of *p-d* and *s-d* interactions in the electronic structure and band gap of $Zn_{1-x}M_xO$ (M = Cr, Mn, Fe, Co, Ni, and Cu): Photoelectron and optical spectroscopy and first-principles band structure calculations

S. J. Gilliland,[1] J. A. Sans,[1] J. F. Sánchez-Royo,[1] G. Almonacid,[1] B. García-Domene,[1] A. Segura,[1] G. Tobias,[2] and E. Canadell[2]

[1]*MALTA-Consolider Team, Institut de Ciència dels Materials-Dpto. de Física Aplicada, Universitat de València, E-46100 Burjassot (València), Spain*

[2]*Institut de Ciència de Materials de Barcelona (ICMAB-CSIC), Campus de la UAB, 08193 Bellaterra, Barcelona, Spain*

(Received 19 July 2012; published 2 October 2012)

We report an investigation on the effect of *p-d* and *s-d* interactions in the electronic structure, and especially in the band-gap value, of wurtzite wide-gap diluted magnetic semiconductors $Zn_{1-x}M_xO$ (M = Cr, Mn, Fe, Co, Ni, Cu). Thin films prepared by pulsed laser deposition are investigated by means of optical absorption at low-temperature and photoelectron spectroscopy. Pure wurzite phase is shown to be maintained for Co and Mn concentrations up to 25% and for Cr up to 10%, while in the case of Fe, Ni, and Cu, other phases are present for concentrations higher than 5, 2, and 1%, respectively. The band gap of the $Zn_{1-x}M_xO$ alloy increases at a rate of 9, 22, 4, and 23 meV/%M for M = Cr, Mn, Fe, and Co, respectively, and decreases at a rate of about −14 and −10 meV/%M for M = Ni and Cu. Photoelectron spectroscopy of the $Zn_{1-x}M_xO$ valence band for M = Mn and Co shows that the emergence of the transition metal-related photoemission peak is clearly correlated to a larger binding energy of the O 2*p* valence-band peaks. A simple model of *p-d* and *s-d* interaction is proposed in which the decrease of Zn 3*d* electron density below the valence band and the increase of M 3*d* electron density for M = Cr to Co lead to higher binding energies of the valence-band maximum and, thus, to a larger band gap. In contrast, for Ni and Cu the 3*d* electrons lie below the valence-band maximum and push it to lower binding energies, thus decreasing the band gap. This simple model is basically confirmed by first-principles density functional theory band structure calculations. Detailed analyses of the band structures and densities of states show that the *p-d* interaction leads to an increase of the band gap for M = Mn to Co but a decrease for M = Ni and Cu. They also suggest that the *s-d* interaction plays the major role or contributes as much as the *p-d* interaction in leading to the increase of the band gap for M = Cr and Mn, respectively.

DOI: 10.1103/PhysRevB.86.155203 PACS number(s): 75.50.Pp, 78.66.Hf, 71.15.Mb, 71.35.Cc

I. INTRODUCTION

In spite of the large amount of literature on the optical properties of ZnO-based diluted magnetic semiconductors (DMS) like $Zn_{1-x}M_xO$ (M = Cr, Mn, Fe, Co, Ni, Cu), there are apparently contradictory results concerning their band-gap dependence on the transition metal (TM) proportion. The case of $Zn_{1-x}Co_xO$ seems to be the most controversial one. Based on careful photoluminescence,[1] reflectivity[1] and absorption measurements,[2–4] there is strong experimental evidence that the band gap of $Zn_{1-x}Co_xO$ increases with the Co content, even at a larger rate than it would be expected from the relatively small decrease of the atomic number when replacing Zn by Co. Nevertheless some authors report a band-gap decrease as the Co content increases.[5–8] This result is based on transmission measurements on thin films with thicknesses larger than some 300 nm that are sensitive only to the low-energy tail of the charge transfer (CT) absorption band. The onset of the CT band is mistakenly identified as the fundamental valence-to-conduction band transition.

In the case of $Zn_{1-x}Mn_xO$, the lower intensity of the CT absorption band, appearing at lower photon energy and more clearly separated from the fundamental edge, has been correctly identified by most authors, and there is a clear consensus on the large increase of the band gap as the Mn content increases.[9–11]

For $Zn_{1-x}Fe_xO$ the situation is confusing as some papers report an increase of the band gap,[12,13] while some others report a decrease[14,15] as the Fe content increases. Only Ref. 15 reports full dielectric function spectra as obtained through spectroscopic ellipsometry. Even if the exciton peak in the dielectric function imaginary part remains visibly at the same energy independently of the Fe proportion, the authors report a band-gap decrease. This is also the case of $Zn_{1-x}Cr_xO$, for which Yilmaz *et al.*[16] report a band-gap decrease of about 100 meV for a 4.6% Cr film, even if the donor-bound exciton photoluminescence peak is at a slightly higher energy, as also observed by Liu *et al.*[17] Finally, concerning $Zn_{1-x}Ni_xO$[18] and $Zn_{1-x}Cu_xO$,[19,20] there seems to be very few results on their optical properties, and all authors report a decrease of the band gap as the Ni or Cu concentration increases.

From a physical point of view, the issue is relevant as most models proposed to explain the origin of ferromagnetism in ZnO-based DMS include physical parameters like the carrier effective mass that are directly correlated to the value of the band gap.[21–23] As a general rule, the direct band-gap energy of semiconductors in the wurtzite or zinc-blende structure increases as the average atomic number decreases, as in the series ZnTe, ZnSe, ZnS. This rule has some exceptions, like the lower band gap of ZnO with respect to that of ZnS or the case of copper chalcopyrites, due to *p-d* hybridization between cation 3*d* levels and anion 2*p* levels.[24,25] Following the general trend, it seems reasonable to expect that the substitution of Zn for lighter transition cations (with a lower atomic number) would produce an increase in the band-gap energy of these alloys. Nevertheless, anomalies are to be expected owing to *p-d* hybridization of O 2*p* levels and M cation 3*d* levels.

In this work we present a systematic investigation of the *p-d* interaction in $Zn_{1-x}M_xO$ (M = Cr, Mn, Fe,Co, Ni, and Cu) semiconductor alloys. After describing the experimental methods (Sec. II) and computational details (Sec. III), we will present the experimental results (Sec. IV) and discuss them initially on the basis of a simple *p-d* and *s-d* interaction model (Sec. V A) and then on the basis of first-principles band structure calculations (Sec. V B). As it will be shown, the *s-d* interaction must also be taken into account for substitution with the lighter Cr and Mn elements.

II. EXPERIMENTAL METHOD

$Zn_{1-x}M_xO$ (M = Cr, Mn, Fe, Co, Ni, and Cu) films with nominal concentrations varying between 0.5 and 25%, depending on the solubility of the dilute cation, were deposited over sapphire and mica substrates by pulsed laser deposition in the system described in Ref. 26. Targets were formed from compressed pellets containing a mixture of ZnO and the dilute cation oxide in stoichiometric proportions, which were baked in an oven at 1250 K for 12 h in an air atmosphere. The substrate temperature was 600 °C and an oxygen pressure of 2×10^{-5} mbar was maintained throughout. Films with thicknesses from 80 to 200 nm were used. These films were then structurally characterized by a range of x-ray techniques [x-ray diffraction (XRD) and x-ray absorption (XAS)] to test their quality and the presence, if any, of unwanted phases.

Low-temperature absorption spectra were taken for all DMS samples deposited over sapphire in the spectral range 250 to 700 nm. The sample and a blank sapphire substrate were mounted on the same holder to enable the respective measurements of the sample and direct light spectra, required for normalization purposes. The absorbance and transmittance were measured in the temperature range from 20 to 290 K.

X-ray and ultraviolet photoemission measurements (XPS-UPS) were carried out in a laboratory apparatus and in a synchrotron experiment. In all cases photoemission measurements were performed in $Zn_{1-x}M_xO$/ZnO devices in which the alloy film partially covers the ZnO film deposited on the substrate (as will be seen in the device sketch on top of Figs. 7 and 8). This kind of device has the advantage of allowing for direct comparison of ZnO and $Zn_{1-x}M_xO$ photoelectron spectra acquired in the same conditions. Before these measurements, samples were introduced in the analysis chamber and sputtered by using an Ar^+ gun for 15 min in order to clean the surface. Then, x-ray photoemission measurements were performed to check that the presence of adventitious C on the surface sample was under the detection limit of the experimental setup. All spectra obtained have been referred to the Fermi level.

The laboratory equipment is an ultrahigh-vacuum ESCALAB 210 multianalysis system (base pressure 1.0×10^{-10} mbar) from Thermo VG Scientific. Photoelectrons were excited by means of an Mg anode x-ray source and a Helium lamp by using both the He I (21.2 eV) and He II (40.8 eV) excitation lines.

XPS-UPS synchrotron experiments were carried out at the ANTARES beamline in SOLEIL synchrotron. All photoemission results reported here were measured by using a photon energy ($h\nu$) $h\nu$<65 eV. The Fermi level was determined by measuring the Fermi edge in the Cu sample holder in electrical contact with the sample.

III. COMPUTATIONAL DETAILS

Band structure calculations were carried out using a numerical atomic orbitals density functional theory (DFT)[27] approach, which has been developed and designed for efficient calculations in large systems and implemented in the Spanish Initiative for Electronic Simulations with Thousands of Atoms (SIESTA) code.[28–30] We have used the generalized gradient approximation to DFT and, in particular, the functional of Perdew, Burke, and Ernzerhof.[31] Only the valence electrons are considered in the calculation, with the core being replaced by norm-conserving scalar relativistic pseudopotentials[32] factorized in the Kleinman-Bylander form.[33] Nonlinear partial-core corrections to describe the exchange and correlations in the core region were used for Zn, Mn, Fe, Co, Ni, and Cu.[34] We have used a split-valence double-ζ basis set, including polarization orbitals for all atoms.[35] The 3*d* electrons of Zn were treated as valence electrons. For Zn we have used a pseudopotential generated using a Zn^{2+} reference configuration[36] and an optimized basis set.[37] The crystallographic parameters for ZnO obtained in such way (a = 3.300 Å, c = 5.297 Å, u = 0.381) are in good agreement with the more accurate plane-wave-type DFT calculations presently available[38] (a = 3.282 Å, c = 5.291 Å, u = 0.379) as well as with the experimental structure[39] (a = 3.250 Å, c = 5.200 Å, u = 0.382). All calculations were carried out using a $3 \times 3 \times 2$ supercell in which one of the Zn atoms is substituted by a TM atom, which corresponds to a substitution degree close to 2.8%. All structures were fully optimized. Because of the presence of TM atoms with open-shell configurations, our calculations are of the spin-polarized type. However, since our main interest is in the evolution of the optical gap as the nature of the TM atom changes, we have not made any attempt to look at different magnetic configurations of the materials. It is already known that even using smaller supercells (and thus higher TM concentrations), the calculated energy differences can hardly be considered as significant.[36] The energy cutoff of the real-space integration mesh was 1600 Ry. The Brillouin zone was sampled using grids of $(2 \times 2 \times 2)$ and $(10 \times 10 \times 10)$ k points for structural optimizations and density of states (DOS) analysis, respectively.[40] We checked that the results are well converged with respect to the real-space grid, the Brillouin zone sampling, and the range of the numerical atomic orbitals.

IV. EXPERIMENTAL RESULTS

A. Structural measurements

Site configuration of M cations in ZnO was investigated by XAS experiments. XAS near-edge structure (XANES) spectra at the K edge of the different TMs were recorded for increasing concentrations and compared to XANES spectra at the Zn K edge. $Zn_{1-x}Co_xO$ and $Zn_{1-x}Mn_xO$ thin films keep the wurtzite structure, with Co (Mn) in Zn substitutional sites up to the M content of the order of 25%.[41–44] For $Zn_{1-x}Fe_xO$, single wurtzite phase with Fe in the substitutional Zn site is kept only for Fe concentrations below 5%, while for $Zn_{1-x}Ni_xO$ and $Zn_{1-x}Cu_xO$, Ni and Cu are in substitutional sites only

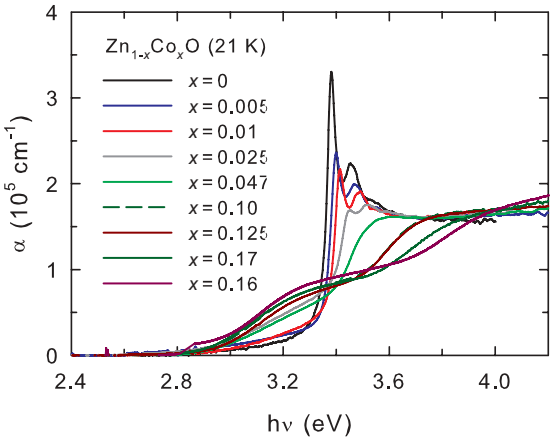

FIG. 1. (Color online) Optical absorption edge of $Zn_{1-x}Co_xO$ thin films for different Co content.

for concentrations below 2 and 1%, respectively. For higher concentrations the XANES spectra at Ni (Cu) K edges show that most of the Ni (Cu) is segregated from the ZnO film in NiO (Cu_2O) crystallites.

XRD spectra show that the thin films studied here grow in the (0001) direction. XRD spectra do not show any trace of extra phases for $Zn_{1-x}Cr_xO$ and $Zn_{1-x}Co_xO$ films. Small traces of extra phases appear in $Zn_{1-x}Mn_xO$ for $x = 0.25$. Consistently with XAS results, XRD peaks of extra phases are observed in $Zn_{1-x}Fe_xO$, $Zn_{1-x}Ni_xO$, and $Zn_{1-x}Cu_xO$ for $x > 0.05$, 0.02, and 0.01, respectively. Consequently, the only results that we will discuss in this work refer to those thin films in which the M cation is in tetrahedral substitutional sites.

B. Optical measurements

Figures 1 to 4 show the absorption spectra at 21 K of $Zn_{1-x}M_xO$ thin films for M = Co (Fig. 1), Mn (Fig. 2), Fe [Fig. 3(a)], Cr [Fig. 3(b)] Ni [Fig. 4(a)], and Cu [Fig. 4(b)]. In every figure the absorption of a pure ZnO thin film prepared in the same conditions[26] is also shown. The exciton peak corresponds to the B exciton, with perhaps some contribution of the A exciton (a well-resolved A exciton peak is

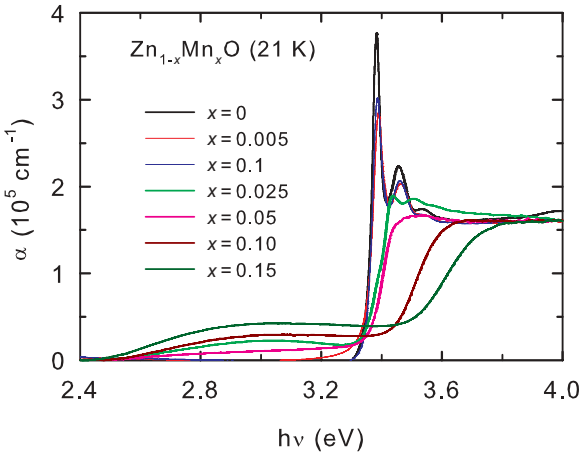

FIG. 2. (Color online) Optical absorption edge of $Zn_{1-x}Mn_xO$ thin films for different Mn content.

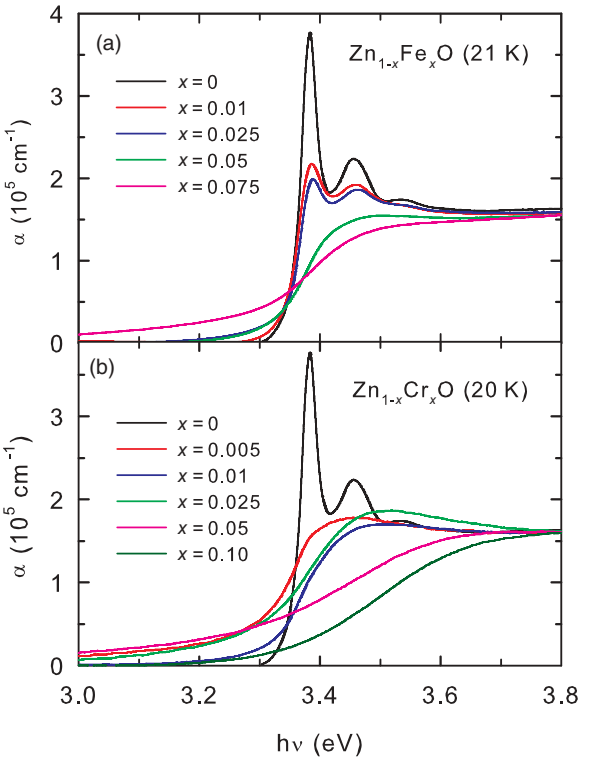

FIG. 3. (Color online) Optical absorption edge of $Zn_{1-x}Fe_xO$ (a) and $Zn_{1-x}Cr_xO$ (b) thin films for different Fe and Cr contents.

observed only in epitaxial ZnO films grown on lattice-matched substrates as $ScAlMgO_4$).[45] The peaks at higher photon energies correspond to exciton + LO and exciton + 2LO polar

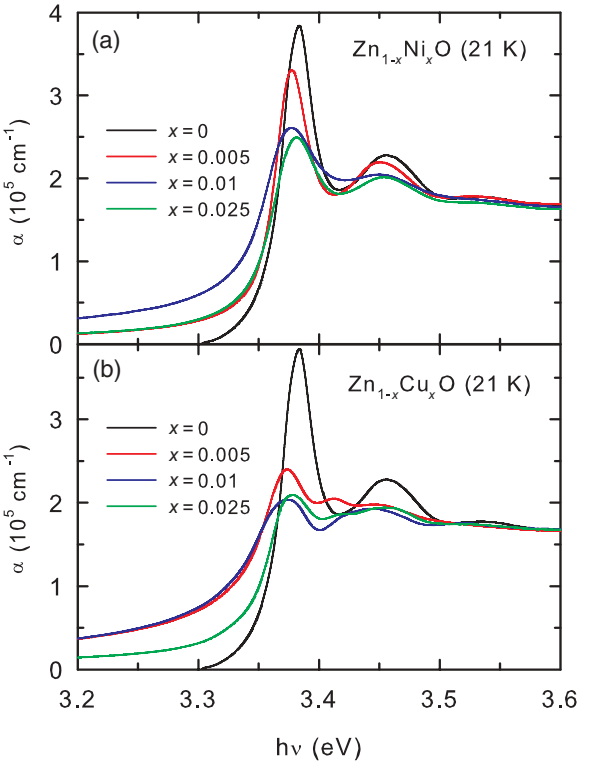

FIG. 4. (Color online) Optical absorption edge of $Zn_{1-x}Ni_xO$ (a) and $Zn_{1-x}Cu_xO$ (b) thin films for different Ni and Cu contents.

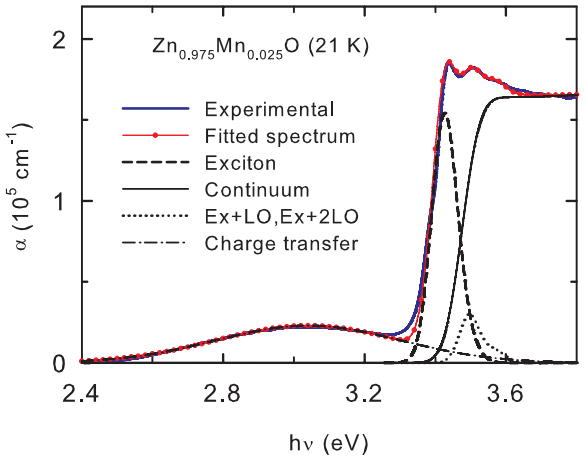

FIG. 5. (Color online) Example of Elliot-Toyozawa fit to the experimental absorption edge of $Zn_{1-x}Mn_xO$ ($x = 0.025$) and showing the components of the fitted spectrum.

phonon resonances.[26] As mentioned above, all spectra shown in Figs. 1–4 correspond to those for M concentrations yielding pure wurtzite phases.

For Mn and Co the fundamental absorption edge is partially overlapped by a broad absorption band, the intensity of which is clearly correlated to the Mn or Co content, that has been ascribed to a charge transfer transition (CTT) from the fundamental state of the M $3d$ shell to the semiconductor alloy conduction band.[2,3,11,46] No similar CTT absorption band, clearly correlated to the M content, has been detected for Cr, Fe, Ni, or Cu. For low M content (except for $Zn_{1-x}Cr_xO$, for which only a broad maximum appears), the exciton and exciton $+$LO polar phonon peaks are clearly observed and unambiguously show the tendency of the gap change as a function of the M content. Clearly, the band gap of the alloy increases with increasing the M content for Cr, Mn, Fe, and Co and decreases with increasing the M content for Ni and Cu.

In order to extract quantitative information about the band-gap variation, the absorption edge was interpreted through the Elliot-Toyozawa model for the exciton discrete and continuum states,[47,48] with a supplementary Gaussian band for the CTT. Figure 5 shows an example of fit for $Zn_{0.975}Mn_{0.025}O$ at 20 K. From this fitting procedure, the value of the alloy band gap and the transition width can be obtained. The transition width increases with the M concentration, as expected from the increase of the alloy disorder scattering. Here, we will focus on the band gap of $Zn_{1-x}M_xO$ as a function of the different M atomic proportion, as shown in Fig. 6. Table I shows the band gap versus composition coefficients for the different alloys (slope dE_g/dx of Fig. 6 graphics in electron volts per percent M). Similar band-gap coefficients for $Zn_{1-x}Mg_xO$[49] and $Zn_{1-x}Cd_xO$[50,51] are also given for comparison. As results are ordered according to increasing M atomic numbers, two important features should be stressed: first, the absence of a monotonic dependence of the band-gap coefficient absolute value on the atomic number and, second, the sign change of this coefficient between Co and Ni. It is worth stressing that the slope does not follow the usual trend of larger values for lighter substituting elements. In fact, the largest positive

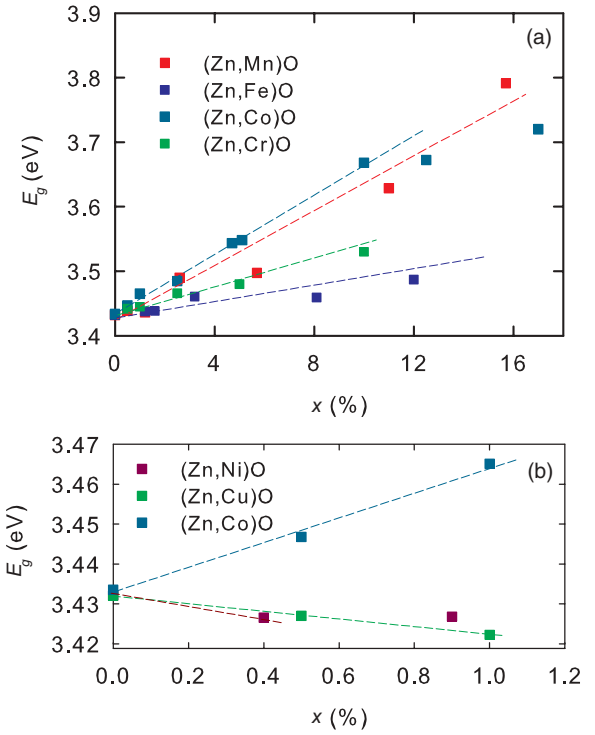

FIG. 6. (Color online) (a) Band gap of $Zn_{1-x}M_xO$ semiconductor alloy thin films as a function of the M content for $M =$ Cr, Mn, Fe, and Co; (b) *idem* for $M =$ Co, Ni, and Cu.

slopes (Co and Mn) are close to that of a much lighter element like Mg, and the largest absolute value of negative slopes is close to that corresponding to a much heavier element like Cd.

C. Photoemission measurements

Figures 7 and 8 show the UPS spectra of the valence band for $Zn_{1-x}Mn_xO$ and $Zn_{1-x}Co_xO$ [red (dark gray) curves], respectively, as well as for the ZnO thin film on which the alloy films have been deposited (black curves). The photon energy used was $h\nu = 40.8$ eV, which allows us to probe states of the ZnO band structure close to the Γ point of the Brillouin zone. They have been vertically displaced relative to each other to allow for comparison.

In all spectra, the characteristic ZnO-related photoemission signals coming from Zn $3d$ and O $2p$ states can be observed.[52] Comparing the spectra measured for ZnO and the alloy films, it can be seen that Mn or Co incorporation into the ZnO lattice reduces the intensity of the Zn $3d$ peak without producing any appreciable energy shift. This is consistent with the expected substitutional role of divalent Co atoms introduced in ZnO.[42]

However Mn or Co incorporation noticeably alters the alloy photoemission spectrum in the proximity of the O $2p$ band lower binding energy edge: a broad structure can be detected at the low binding energy edge of the O $2p$ band, which develops when the Mn or Co content increases. A clearer view of the effect of Mn (Co) incorporation is shown through the difference spectra, intercalated below each pair of $Zn_{1-x}M_xO$/ZnO spectra. Difference spectra were calculated by subtracting the spectrum measured in a ZnO film to that

TABLE I. Band-gap coefficients $Zn_{1-x}M_xO$ alloys as a function of the proportion of the extra ion M.

Cation	Cr	Mn	Fe	Co	Ni	Cu	Mg	Cd
$\frac{dE_g}{dx}$(meV/%M) (experimental)	9	22	4	23	−14	−9.8	23[a]	−15[b]−50[c]
$\frac{dE_g}{dx}$(meV/%M) (first principles)	−21	34	17	14	−41	−39		
$E_{s-d}^{\mathrm{CBM}-M} - E_{p-d}^{\mathrm{VBM}-M}$(eV)	0–0.2	1.3–1.5	−(0.3–0.5)	1.4–1.6	−(2.1–2.3)	−(1.7–1.9)		

[a]Reference 49;
[b]Reference 50;
[c]Reference 51.

measured in the corresponding alloy film of the same device. These difference spectra can be decomposed in three lobes: two-edge lobes of positive intensity and another (the central one) with negative intensity. The absolute intensity of these lobes increases with the Mn (Co) content, although the positive lobe located at lower binding energies dominates the difference spectra, and it is the only lobe clearly detectable at lower Mn (Co) concentration. We have fitted these peaks to three Gaussian curves, of intensity A, B, and C, in going from low to high binding energy. The results of this fitting, which reproduce the difference curves, indicate that the main lobe (that at lower binding energy) is centered about 2.8 eV for $Zn_{1-x}Mn_xO$ and 3.2 eV for $Zn_{1-x}Co_xO$ irrespective of the Mn (Co) content, and its intensity is clearly correlated with the

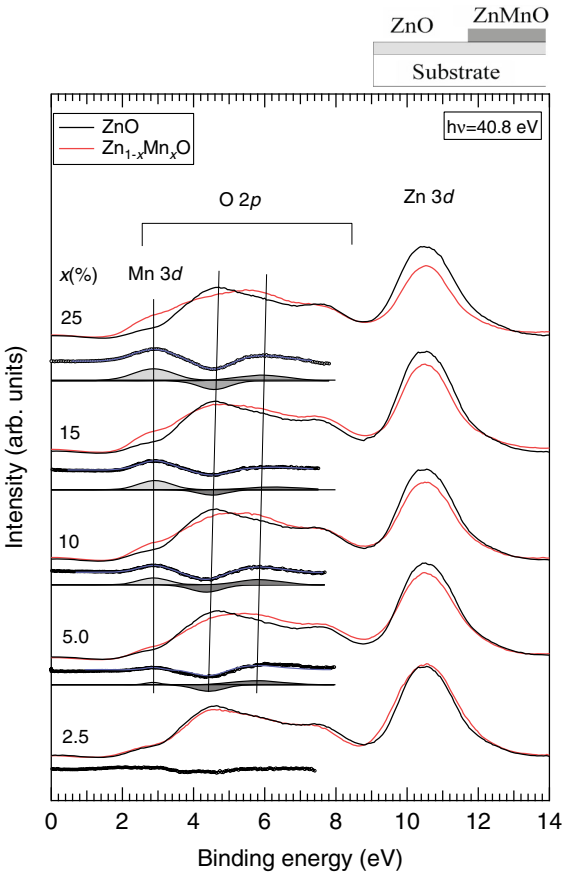

FIG. 7. (Color online) Valence-band photoemission spectra measured in $Zn_{1-x}Mn_xO$ [red (dark gray) curves] and ZnO (black curves) films of $Zn_{1-x}Mn_xO$/ZnO devices as those illustrated at the top of the figure. The Mn content of the corresponding $Zn_{1-x}Mn_xO$ film is indicated on top of the pair of spectra measured in each device. Under each pair of spectra, the difference between the $Zn_{1-x}Mn_xO$ and ZnO spectra is shown (thick black), along with the three-Gaussian peak fittings of these difference curves. Blue (medium gray) solid lines correspond to the sum of the three Gaussian peaks obtained from each fitting.

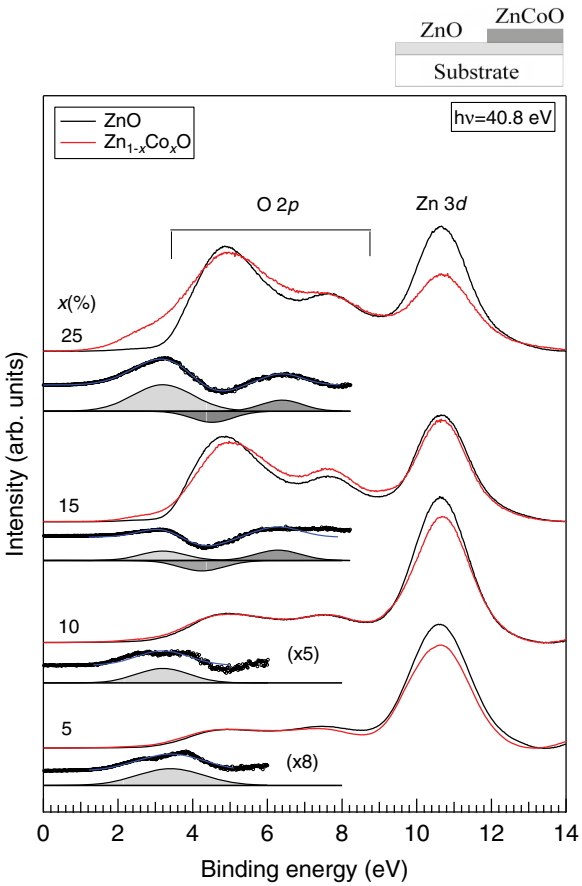

FIG. 8. (Color online) Valence-band photoemission spectra measured in $Zn_{1-x}Co_xO$ [red (dark gray) curves] and ZnO (black curves) films of $Zn_{1-x}Co_xO$/ZnO devices as those illustrated at the top of the figure. The Co content of the corresponding $Zn_{1-x}Co_xO$ film is indicated on top of the pair of spectra measured in each device. Under each pair of spectra, the difference between the $Zn_{1-x}Co_xO$ and ZnO spectra is shown (thick black), along with the three-Gaussian peak fittings of these difference curves. Blue (medium gray) solid lines correspond to the sum of the three Gaussian peaks obtained from each fitting.

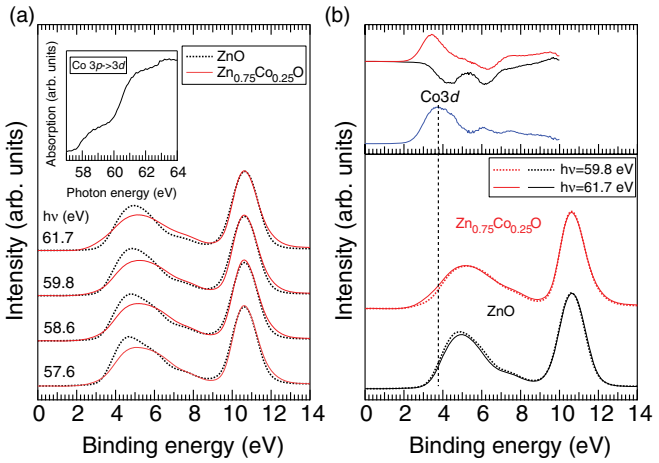

FIG. 9. (Color online) (a) Valence-band resonant photoemission spectra measured at both sides of the Co $3p \rightarrow 3d$ transition in $Zn_{0.75}Co_{0.25}O$ [red (dark gray) curves] and ZnO (black curves) films of one of our devices. The inset shows the absorption spectrum of this transition recorded in the total electron yield mode. The spectra have been acquired in off-resonance conditions (spectra measured with $h\nu < 60.0$ eV) and in on-resonance conditions (spectra measured with $h\nu = 61.7$ eV). (b) Bottom panel: comparison between on- and off-resonance valence-band spectra measured in $Zn_{0.75}Co_{0.25}O$ and in ZnO films with $h\nu$ values close to the transition. Top panel: difference between on- and off-resonance spectra measured in the $Zn_{0.75}Co_{0.25}O$ [red (dark gray) curve] and in the ZnO (black curve) films. The difference curve obtained by subtracting these two curves is plotted at the bottom [blue (medium gray) line].

Mn (Co) content. The middle and right peaks have a similar intensity ($|B| \approx C$) and can be interpreted as a derivative of the main O $2p$ peak reflecting a shift to lower binding energy. These results indicate that Mn (Co) incorporation into ZnO, does not only introduce Mn (Co)-related states located at the O $2p$ band edge but also modifies the binding energy of the O $2p$ band. We attribute the photoemission signal developing with the Mn (Co) content at around 3 eV as originating from Mn (Co) $3d$ states.

In order to check this hypothesis and to elucidate the origin of this 3 eV peak, we have performed resonant photoemission measurements at both sides of the Co $3p \rightarrow 3d$ transition in the $Zn_{0.75}Co_{0.25}O$ device. This experimental procedure is based on the fact that, by using an appropriate photon energy, it is possible to promote electrons from deep states of an atomic species (i.e., Co $3p$ states) to empty intermediate states of the same species (i.e., Co $3d$ states). Their subsequent relaxation can produce a final state identical to the direct photoemission process, which consequently enhances the valence-band photoemission signal coming from Co $3d$ states. The XAS spectrum measured in this sample [inset of Fig. 9(a)] allows the identification of the Co $3p \rightarrow 3d$ transition, which occurs around $h\nu \approx 60.5$ eV in agreement with previous results.[53] Photoemission spectra shown in Fig. 9(a) were measured with different $h\nu$ off- and on-resonances of the Co $3p \rightarrow 3d$ transition in ZnO and the $Zn_{0.75}Co_{0.25}O$ films. In going from far off- to on-resonance, the spectra measured in the ZnO film appear to exhibit some O $2p$ band dispersion to higher energies, which is indicative of the predominant (001) orientation of the ZnO films, with their c axis normal to the surface. However, for the $Zn_{0.75}Co_{0.25}O$ film, the expected O $2p$ band dispersion with $h\nu$ seems to be masked by the effects of the Co incorporation on the ZnO band structure. In Fig. 9(b) we compare the spectra acquired off-resonance (with $h\nu = 59.8$ eV) and on-resonance (with $h\nu = 61.7$ eV) conditions in both films. The O $2p$ band of the spectra measured at both sides of the transition in the ZnO film exhibits small differences in intensity distribution attributable to band dispersion or dipolar matrix-element effects. In any case, no photoemission-signal enhancement at the low-energy edge of the O $2p$ band is observed. In contrast, the photoemission signal around 3 eV is enhanced in the on-resonance spectrum with respect to the off-resonance one for the $Zn_{0.75}Co_{0.25}O$ film. These results allow us to establish that Co atoms incorporated in these ZnO films introduce Co $3d$ states, rather than defect states, which overlap with the low binding energy edge of the O $2p$ band. The difference between the on- and off-resonance for the $Zn_{0.75}Co_{0.25}O$ film [red (dark gray) curve in the top panel of Fig. 9(b)] would allow us to extract the Co $3d$ partial DOS. However, the spectral weight distribution of the O $2p$ band in pure ZnO exhibits some differences between the spectra measured in off- and on-resonance [Fig. 9(b)], as it can be seen in the difference curve calculated from these spectra [top panel of Fig. 9(b), black curve]. This indicates that a better estimate of the Co $3d$ partial DOS would come from the difference between the two difference curves mentioned above. In this way, the Co $3d$ partial DOS obtained [top panel of Fig. 9(b), blue (medium gray) curve] is dominated by states distributed quasisymmetrically along ± 1 eV from its maximum located at $\sim$4 eV, with a vanishing contribution into the ZnO band gap. The smooth background appearing at the high binding energy side of this Co $3d$ peak may come from additional Co states overlapping with the unavoidable photoemission signal coming from the inelastic scattering of electrons excited from the Co $3d$ states.

Once the origin of the electronic states at 3–4 eV introduced by Co atoms in the ZnO band structure has been discussed, we will face now the question of the source of the changes observed in the spectral weight of the O $2p$ band of ZnO originating from the Mn (Co) incorporation (Figs. 7 and 8). Resonant photoemission results similar to those obtained here have been already reported for $Zn_{1-x}Co_xO$ thin films with a lower Co content.[53–55] In these papers, the enhancement of the photoemission signal in the on-resonance spectra at energies around $\sim$3 eV has been considered to originate from Co $3d$ states. However, the positive lobe observed at high binding energies in the $Zn_{1-x}Co_xO$/ZnO difference spectra (Fig. 8) has been attributed also to Co $3d$ states.[53,55] From our results (Fig. 8), it seems that the appearance of the positive high-energy lobe implies the appearance of the negative one, due to its diametrically opposite evolution with Co content. Moreover, it has been seen that Al codoping of $Zn_{1-x}Co_xO$ enhances the intensities of both negative and positive lobes when compared to that of the lobe assigned to Co $3d$ states.[55] It has been reported that Al dopes ZnO n-type, but the consequent band downshift is lower than that expected by doping-induced band-gap renormalization effects.[52] Therefore, Al codoping of $Zn_{1-x}Co_xO$ would tend to sink Co $3d$ states into the O $2p$

valence band of ZnO. These facts suggest that states with a main O $2p$ orbital origin are involved in the appearance of the negative and high-energy positive lobes, which are perturbed by the introduction of Co $3d$ states. The variation of the O $2p$ spectral weight of ZnO caused by Co incorporation can be explained by the fact that Co atoms, which are in Zn sites, introduce Co $3d$ states in the top of the valence-band maximum (VBM). This produces a double effect on the O $2p$ valence band. On the one hand, the density of Zn atoms diminishes, locally relaxing the on-site potential of O $2p$ states as a consequence of the decrease of the O $2p$−Zn $3d$ repulsion on these states. On the other hand, a new p-d interaction appears between the Co $3d$ located at the low-energy side of the O $2p$ valence band. These two effects tend to push down O $2p$ states from the ZnO VBM and enhance the spectral weight of the O $2p$ band at energies of 6–7 eV.

V. DISCUSSION

A. Simple *p-d* and *s-d* interaction model

In order to discuss the problem of p-d and s-d interaction between the TM d shell and the host electronic states, let us first recall the C_{6v} group representations and their corresponding functions (Table II). ZnO conduction-band minimum (CBM) states at the Γ point belong to the A_1 representation. ZnO VBM consists of three bands (A, B, and C in the standard notation), as a result of crystal field and spin-orbit interaction. In the absence of spin-orbit interaction, at the Γ point the A and B bands form an E_1 doublet, and C is an A_1 singlet lying at lower energy. In perfect tetrahedral coordination (T_d point group), the M $3d$ states split into a lower-energy E doublet state and a higher-energy T triplet. Under the wurtzite structure uniaxial distortion (C_{6v} point group), the lower doublet has E_2 symmetry and the triplet splits into an E_1 doublet and an A_1 singlet. M $3d$ states with A_1 symmetry are expected to interact with the ZnO CBM and C VBM states. M $3d$ states with E_1 symmetry are expected to interact with the ZnO A-B VBM states.

For most semiconductor alloys (with the exception of systems with strong bowing), the band gap follows the common trend of increasing as the mean atomic number decreases. If the band gap of ZnO-based DMS does not follow this trend, the origin of such behavior should lie in some specific feature of the ZnO electronic structure. An outstanding feature of ZnO is the so-called band-gap anomaly (the fact that the band gap of ZnO is smaller than that of ZnS). Since the work of Zunger and coworkers,[24,25,56] it is well known that p-d interaction plays an important role in this ZnO feature. p-d hybridization is allowed in the wurtzite structure due to the lack of inversion symmetry, and, as a consequence, the VBM has some d antibonding character and is shifted to higher energies. The reduction of the p-d interaction when Zn is replaced by an element like Mg, without $3d$ levels, is a relevant contribution to the large band gap versus composition coefficient.[49]

TABLE II. C_{6v} group representations relevant for the discussion.

Representations	p functions	d functions
A_1	z	z^2, x^2+y^2
A_2		
B_1		
B_2		
E_2		(x^2-y^2,xy)
E_1	(x,y)	(xz,yz)

A simple model of p-d and s-d interactions can be built following the ideas put forward by Wei and Zunger in Ref. 24. Matrix elements as well as Zn and M $3d$ shell energies are the relevant parameters. In the case of M elements, the $3d$ shell energy is expected to be above the VBM (mainly with O $2p$ character) for the lighter ones (Cr, Mn, Fe, Co) and below it for the heavier ones (Ni or Cu). Matrix elements $V_{p-d}^{\mathrm{O}-M}$ and $V_{p-d}^{\mathrm{O}-\mathrm{Zn}}$ account for the p-d interaction between Zn $3d$ and O $2p$ on the one side and between M $3d$ and O $2p$ on the other. Also, the s-d interaction between the CBM (mainly with Zn s character) and the A_1 M $3d$ states, is taken into account through the matrix element $V_{s-d}^{M-\mathrm{Zn}}$. The relevant energies of the M $3d$ states correspond to the A_1 and E_1 states. For the sake of simplicity, we neglect the uniaxial C_{6v} crystal field splitting between them and refer to this energy as E_{M3d}. With these assumptions, the CBM and VBM shifts in $\mathrm{Zn}_{1-x}M_x\mathrm{O}$ alloys when p-d and s-d interactions are considered, can be described by the following equations:[24]

$$E_{\mathrm{CBM}}^{\mathrm{alloy}} = E_{\mathrm{CBM}}^{no\,spd} + \frac{\left|V_{s-d}^{M-\mathrm{Zn}}\right|^2}{E_{\mathrm{CBM}}^{no\,spd} - E_{M\,3d}}x = E_{\mathrm{CBM}}^{no\,spd} + E_{s-d}^{\mathrm{CBM}-M}x$$

$$E_{\mathrm{VBM}}^{\mathrm{alloy}} = E_{\mathrm{VBM}}^{no\,spd} + \frac{\left|V_{p-d}^{\mathrm{O}-\mathrm{Zn}}\right|^2}{E_{\mathrm{VBM}}^{no\,spd} - E_{\mathrm{Zn}\,3d}}(1-x) + \frac{\left|V_{p-d}^{\mathrm{O}-M}\right|^2}{E_{\mathrm{VBM}}^{no\,spd} - E_{M3d}}$$

$$= E_{\mathrm{VBM}}^{no\,spd} + E_{p-d}^{\mathrm{VBM}-\mathrm{Zn}}(1-x) + E_{p-d}^{\mathrm{VBM}-M}x \qquad (1)$$

where second-order perturbation terms are reduced to energy parameters describing the intensity of s-d ($E_{s-d}^{\mathrm{CBM}-M}$) and p-d ($E_{p-d}^{\mathrm{VBM}-\mathrm{Zn}}$, $E_{p-d}^{\mathrm{VBM}-M}$) interactions, whose signs depend on the relative position of M $3d$ states with respect to CBM and VBM. The alloy band gap, modified by s-d and p-d interactions, would then be given by the following equation:

$$E_g^{\mathrm{alloy}} = E_{\mathrm{CBM}}^{\mathrm{alloy}} - E_{\mathrm{VBM}}^{\mathrm{alloy}} = E_g^{\mathrm{ZnO},\,no\,spd} - E_{p-d}^{\mathrm{VBM}-\mathrm{Zn}}(1-x) + \left(E_{s-d}^{\mathrm{CBM}-M} - E_{p-d}^{\mathrm{VBM}-M}\right)x. \qquad (2)$$

The band gap versus composition coefficient would then be

$$\frac{dE_g^{\mathrm{alloy}}}{dx} = E_{p-d}^{\mathrm{VBM}-\mathrm{Zn}} + \left(E_{s-d}^{\mathrm{CBM}-M} - E_{p-d}^{\mathrm{VBM}-M}\right). \qquad (3)$$

An estimation of the energy $E_{p-d}^{\mathrm{VBM}-\mathrm{Zn}}$ can be obtained from the VBM offset in $\mathrm{Zn}_{1-x}\mathrm{Mg}_x\mathrm{O}$ alloys, as Mg has no $3d$ occupied states. The distribution of the total band-gap increase between the CBM and VBM offsets (as described by the ratio $\Delta E_C/\Delta E_V$) is controversial. and ratio values as large as 90/10, assigning most of the offset to the CBM, have been proposed.[57,58] Given the well-established role of p-d interaction in the ZnO band-gap anomaly,[24] such a low VBM offset is unlikely. Coli and Bajaj[59] propose a $\Delta E_C/\Delta E_V$ ratio ranging from 60/40 to 70/30 that has been accepted by other authors[60] and seems more consistent with ZnO electronic structure.[61] From the band gap versus composition coefficient for $\mathrm{Zn}_{1-x}\mathrm{Mg}_x\mathrm{O}$ alloys in Table I, $E_{p-d}^{\mathrm{VBM}-\mathrm{Zn}}$ in Eq. (1) should

be between 0.7 and 0.9 eV, a value that is fully consistent with first-principles calculations of p-d interaction in II-VI semiconductors.[24,56] The contribution of $E_{p-d}^{\mathrm{VBM-Zn}}$ to the band gap versus composition coefficients in Table I could then be estimated to be from 7 to 9 meV/%M. On the assumption that band gap versus composition coefficients are only due to p-d and s-d interaction, an estimation of $E_{s-d}^{\mathrm{CBM}-M} - E_{p-d}^{\mathrm{VBM}-M}$ is immediate and is shown in Table I. Let us also recall that the absolute values of $E_{s-d}^{\mathrm{CBM}-M}$ and $E_{p-d}^{\mathrm{VBM}-M}$ are inversely correlated [Eq. (1)]. If we assume that M 3d energies are within ZnO forbidden band, $E_{s-d}^{\mathrm{CBM}-M}$ would dominate for lighter elements (M 3d energies close to the CBM), while $E_{p-d}^{\mathrm{VBM}-M}$ would dominate for heavier elements (M 3d energies close to the VBM).

With these estimations, Eq. (3) qualitatively explains the general trend of the band-gap behavior. For lighter M elements, 3d shell energies are above the O 2p energy and below Zn s energies, the $E_{p-d}^{\mathrm{VBM}-M}$ is negative, and the three terms in Eq. (3) contribute with the same sign. For heavier M elements, 3d states would be at energies just below the VBM. Then, $E_{p-d}^{\mathrm{VBM}-M}$is positive and larger than $E_{p-d}^{\mathrm{VBM-Zn}}$, as $E_{\mathrm{O}2p}$-$E_{M3d} \ll E_{\mathrm{O}2p}$-$E_{\mathrm{Zn}3d}$. This is qualitatively reflected in $E_{p-d}^{\mathrm{VBM}-M}$ values larger for Ni and Cu than for the rest of the elements. This pushes up in energy the VBM, and thus, the band gap decreases.

Nevertheless, this model does not quantitatively explain the relative value of the gap coefficient for light elements. Given that 3d levels are expected to be increasingly deeper from Cr to Co, one should expect a monotonously increasing band-gap coefficient, which is clearly not the case for the values reported in Table I. Thus, in order to make some progress, we must consider in detail the electronic structure of the alloy through first-principles band structure calculations. In doing this we must bear in mind that the use of a supercell approach implicates an ordered substitution and this may not exactly reflect the situation in real samples.

B. First-principles calculations

There are a number of reports concerning the electronic structure of $Zn_{1-x}M_x$O alloys studied through first-principles DFT calculations.[36,55,62–70] However, to the best of our knowledge, the evolution with M of the electronic structure near the band gap for realistically doped alloys of this type has not been discussed in detail. The band dispersion and DOS calculated for $Zn_{1-x}M_x$O (M = Cr, Mn, Fe, Co, Ni, and Cu) will be seen in Figures 11–16. The band structure of pure ZnO in the $3 \times 3 \times 2$ supercell structure is also shown for comparison in Fig. 10. Note that as usual in DFT calculations, the theoretical band gap is smaller than the experimental value (by approximately 2.2 eV). Given the number of bands and the complexity of their dispersion in supercell calculations, the energy scale has been limited to a few electron volts above the CBM and below the VBM in order to make the general trends clearer. Note that although the gap is underestimated, the separation between the A-B and C bands at Γ is correctly described by the present calculations (i.e., 60-meV DFT versus 40-meV experiment).[71]

We will first discuss the electronic structures of alloys in which the M 3d states do not overlap the alloy valence band (i.e., M = Cr, Mn, and Co), which are thus simpler to understand. Of course, the p-d interaction in these alloys should be less intense.

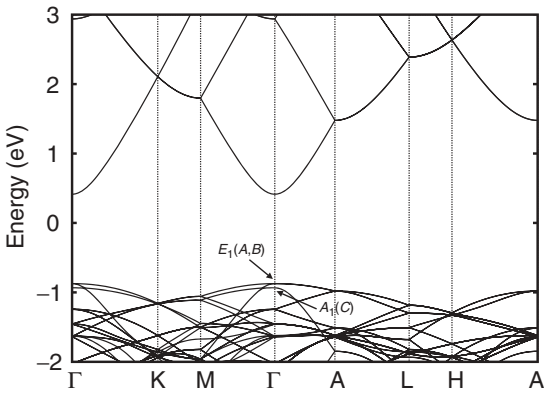

FIG. 10. Band structure of pure ZnO calculated with DFT along various directions of the ZnO Brillouin zone by using a $3 \times 3 \times 2$ supercell. Energy zero refers to the Fermi level.

Concerning the M 3d related DOS peaks in the two cases for which photoemission experiments yield reliable assignments of these peaks, it is relevant to notice that first principles calculations correctly predict their relative energies with respect to the main O 2p DOS peaks in the valence band (about 2 and 1.5 eV for Mn and Co peaks, respectively) [compare Figs. 7 and 12(b) for Mn and Figs. 8 and 13(b) for Co]. These results are a good illustration of the reliability of DFT first-principle calculations for describing occupied states.

Let us start the discussion with the $Zn_{1-x}Cr_x$O electronic structure. The band structure is shown in Fig. 11(a). Clearly, this band structure results from the superposition and weak hybridization of the ZnO band structure (see Fig. 10) and the almost localized levels of Cr. The α-spin Cr E_2 doublet (in the band-gap region) does not exhibit any dispersion (no mixing with valence and conduction bands near the band gap is possible). The α-spin Cr E_1 and A_1 states cross the A_1 alloy conduction band and exhibit also a small dispersion, apart from the expected anticrossing between A_1 states. This anticrossing is the signature of the s-d interaction between Cr 3d states, and the alloy conduction band then pushes down in energy the CBM (s-d repulsion). This is the origin of the sign discrepancy between the experimental and first-principles results in this case and can be easily understood by recalling the usual band-gap underestimation in DFT calculations. α-spin Cr E_1 and A_1 3d states cross the calculated conduction band because, as mentioned before, the DFT calculations underestimate the energy of the conduction band by approximately 2 eV. Once this limitation is considered, in the actual electronic structure the α-spin Cr E_1 and A_1 3d states should also be in the band gap, some 1 eV below the CBM. As a consequence, s-d repulsion would shift the alloy conduction band to higher energies, thus resulting in a positive band-gap coefficient.

The electronic structure of $Zn_{1-x}Mn_x$O [Fig. 12(a)] is not basically different from that of $Zn_{1-x}Cr_x$O apart from the fact that the α-spin Mn E_1 and A_1 3d states are at a lower energy, very close to the CBM, giving rise to a strong anticrossing

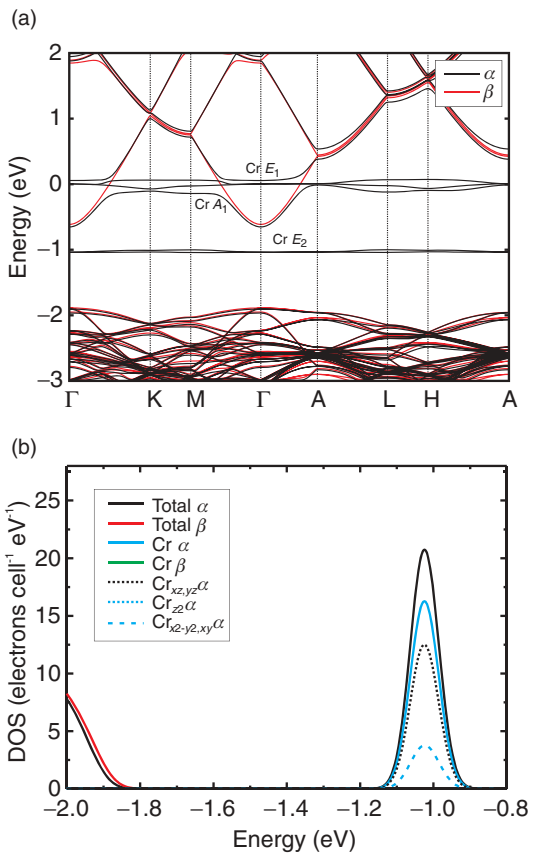

FIG. 11. (Color online) Band structure of $Zn_{0.972}Cr_{0.028}O$ calculated with DFT along various directions of the ZnO Brillouin zone by using a $3 \times 3 \times 2$ supercell. Energy zero refers to the highest occupied level. (b) Valence-band DOS and selected projected DOS contributions of $Zn_{0.972}Mn_{0.028}O$ corresponding to the band structure shown in (a).

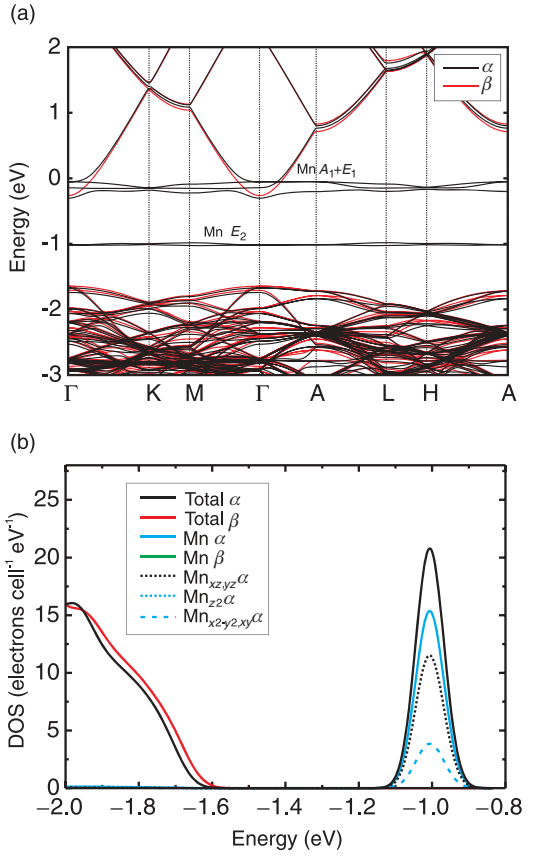

FIG. 12. (Color online) (a) Band structure of $Zn_{0.972}Mn_{0.028}O$ calculated with DFT along various directions of the ZnO Brillouin zone by using a $3 \times 3 \times 2$ supercell. Energy zero refers to the highest occupied level. (b) Valence-band DOS and selected projected DOS contributions of $Zn_{0.972}Mn_{0.028}O$ corresponding to the band structure shown in (a).

between the A_1 $3d$ state and the CBM. The α-spin Mn E_2 doublet is also in the band-gap region and does not exhibit any dispersion (no mixing with valence and conductions bands near the band gap is possible). The α-spin E_1 doublet exhibits some dispersion in directions Γ-M and A-L, indicating some mixing with O $2p_x$-p_y E_1 states in the VBM. However, this mixing seems to be weak given the small Mn $3d$ contribution to the valence-band DOS. This would give rise to a small p-d repulsion lowering the energy of the VBM and then slightly increasing the band gap (with respect to pure ZnO). Then the stronger effect in the band structure of $Zn_{1-x}Mn_xO$ near the gap seems to be the s-d interaction between the A_1 Mn $3d$ singlet and the A_1 alloy conduction band. Globally, both effects lead to a band-gap increase of about 90 meV, which would result in a band-gap coefficient of some 34 meV/%Mn. If the DFT band-gap underestimation is taken into account, the s-d and p-d repulsion effects would be of the same order, both contributing to the band-gap increase.

In the case of $Zn_{1-x}Co_xO$, the occupied α-spin Co $3d$ states are much closer to the VBM [Fig. 13(a)]. The lowest-energy E_2 doublet does not exhibit any dispersion, as expected, but the E_1 doublet exhibits quite strong dispersion in the Γ-M and A-L directions as well as the A_1 singlet in direction Γ-A. This indicates stronger p-d mixing with respect to $Zn_{1-x}Mn_xO$, as reflected by the larger Co $3d$ contribution to the valence-band DOS [Fig. 13(b)]. This "p-d repulsion" results in an increase of the A-B band gap of 14 meV/%Co. The strong mixing of the Co $3d_{z^2}$ A_1 singlet with the A_1 O $2p_z$ VBM results in a clear increase of the crystal field splitting between A, and B and C VBMs. The C band gap would increase by more than 40 meV/% Co. It must be stressed that this kind of effect is a result of the artificial symmetry of the ordered alloy built for supercell calculations, in which each band preserves its own symmetry. The MA_1 $3d_{z^2}$ singlet state mixes only with O A_1 $2p_z$ band. This strong interaction leads to an increase of the uniaxial crystal field splitting between O $2p_x$-p_y and $2p_z$ states that is not actually observed in real films.

In the rest of the alloys (M: Fe, Ni, Cu), the p-d mixing is more relevant, leading to larger dispersion of the M-related states close to or inside the valence band. This adds a supplementary difficulty to the identification of the alloy VBM at the Γ point. General trends can be detected in Fig. 14 (Cu), Fig. 15 (Ni), and Fig. 16 (Fe). As the occupied M $3d$ states enter the alloy valence band, the associated bands present larger dispersion and the corresponding DOS peaks become larger and more intense. Again, it is important to notice that the electronic structure of the ordered alloy exhibits features that do not exist in the real disordered alloy. In particular,

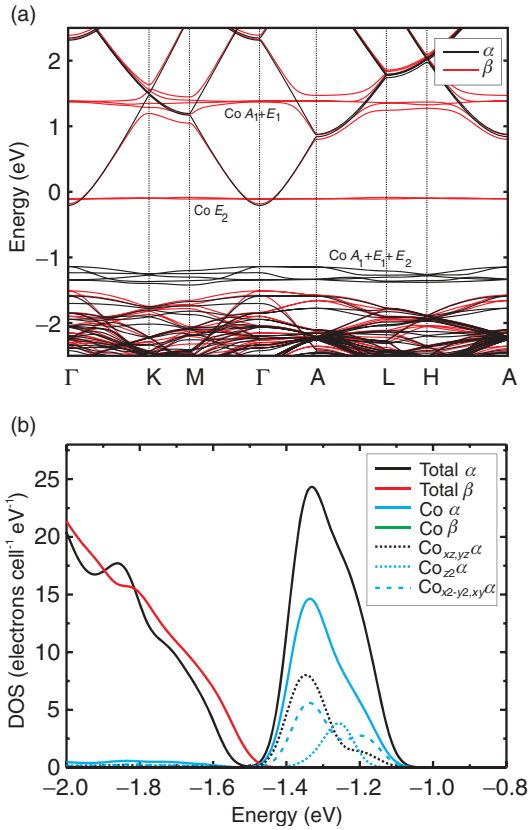

FIG. 13. (Color online) (a) Band structure of $Zn_{0.972}Co_{0.028}O$ calculated with DFT along various directions of the ZnO Brillouin zone by using a $3 \times 3 \times 2$ supercell. Energy zero refers to the highest occupied level. (b) Valence-band DOS and selected projected DOS contributions of $Zn_{0.972}Co_{0.028}O$ corresponding to the band structure shown in (a).

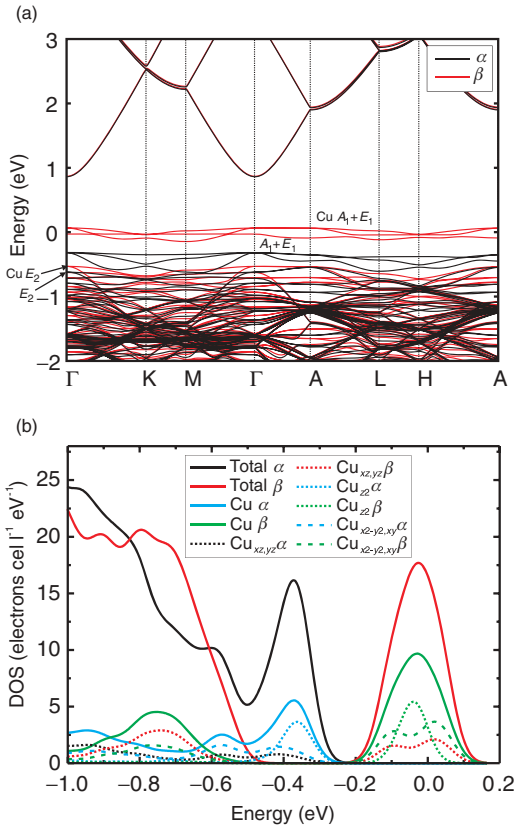

FIG. 14. (Color online) (a) Band structure of $Zn_{0.972}Cu_{0.028}O$ calculated with DFT along various directions of the ZnO Brillouin zone by using a $3 \times 3 \times 2$ supercell. Energy zero refers to the highest occupied level. (b) Valence-band DOS and selected projected DOS contributions of $Zn_{0.972}Cu_{0.028}O$ corresponding to the band structure shown in (a).

given the symmetry of M $3dE_1$ and A_1 states, they mix with O $2pE_1$ (p_x, p_y) and A_1 (p_z) states, giving rise to a set of three α-spin bands appearing in the upper part of the alloy valence band and strongly interacting with the rest of bands (this is especially clear through the strong anticrossing effects visible in the dispersion of A_1 bands along the $\Gamma - A$ direction). Consequently, as discussed for $Zn_{1-x}Co_xO$, the wurtzite crystal field splitting between the A and B and C valence bands can be strongly modified in the ordered alloy. As M $3d$ states become deeper, the orbital composition of the three upper α-spin bands evolves from predominantly M $3d$ (Fe) to predominantly O $2p$ (Cu).

Let us first discuss the case of $Zn_{1-x}Cu_xO$ (Fig. 14), for which the DOS shows [Fig. 14(b)] shows the strongest component of M $3d$ states inside the valence band of the whole series. Cu $3d$ β-spin states appear to be distributed in two DOS peaks, one near the Fermi level (that should originate mainly from Cu $3dE_1$ and A_1 states) another centered at around -0.75 eV (mainly from Cu $3dE_2$). From the dispersion of the highest energy state and the orbital composition, it is clear that even β-spin $3d$ states are hybridized with β-spin O $2p$ states. Nevertheless, the strongest p-d mixing occurs for α-spin Cu $3d$ states, that are all in the valence band and contribute to the DOS from -1.8 to -0.2 eV. As for the α-spin states, the DOS band at -1 eV should come from E_2 states, and the double band between -0.6 and -0.2 eV should come from E_1 and A_1 states, but in this case the Cu-related component spreads along the valence band. This is a clear signature of Cu-O bonding with the subsequent formation of bonding and antibonding states. The fact that Cu $3d$ does not dominate the DOS peak around -0.4 indicates that this corresponds to the VBM, with a strong component of Cu $3d_{z^2}$ (A_1), but very low contribution of the other Cu $3d$ states. The strong mixing between the A_1 Cu $3d$ states and the strongly dispersing A_1 O $2p_z$ (along the $\Gamma - A$ direction) gives rise to the anticrossings that strongly modify the shape of pure ZnO bands near the VBM and, in this case, gives rise to a vanishing wurtzite crystal field. Once the alloy VBM is identified, we can calculate the band-gap change coefficient that turns out to be -39 meV/%Cu.

In the case of $Zn_{1-x}Ni_xO$ (Fig. 15), none of the β-spin states overlap the alloy valence band. All of them present very low dispersion [Fig. 15(a)], and the orbital composition indicates strong Ni character [Fig. 15(b)]. Concerning the α-spin states, the Ni $3d$ contributions to the DOS overlap each other but not as much as in $Zn_{1-x}Cu_xO$, indicating lower p-d mixing. In addition, the highest energy α-spin DOS peak has a larger contribution of Ni states and, contrary to what happens in $Zn_{1-x}Cu_xO$, there is no contribution of Ni $3d_{z^2}$. The Ni $3d_{z^2}$ contribution appears at lower energies (-1.45 eV) and spreads over a larger energy range, indicating a strong hybridization

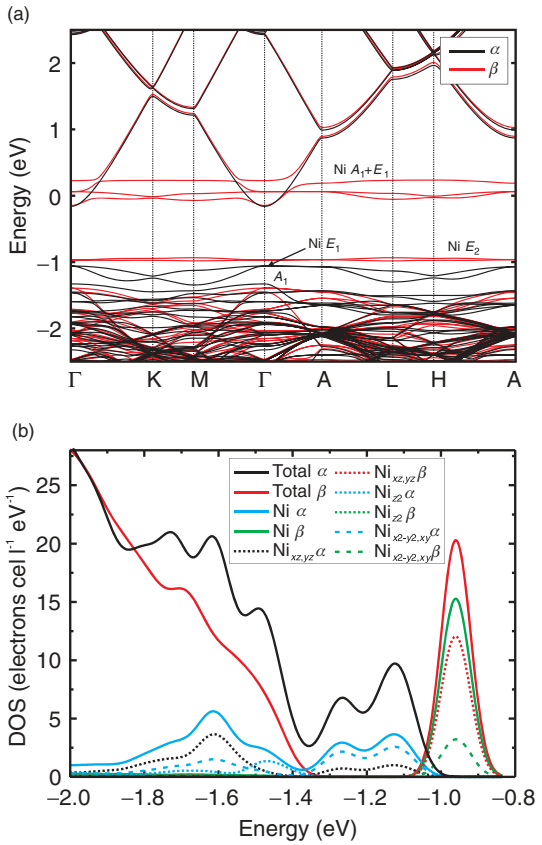

FIG. 15. (Color online) (a) Band structure of $Zn_{0.972}Ni_{0.028}O$ calculated with DFT along various directions of the ZnO Brillouin zone by using a $3 \times 3 \times 2$ supercell. Energy zero refers to the highest occupied level. (b) Valence-band DOS and selected projected DOS contributions of $Zn_{0.972}Ni_{0.028}O$ corresponding to the band structure shown in (a).

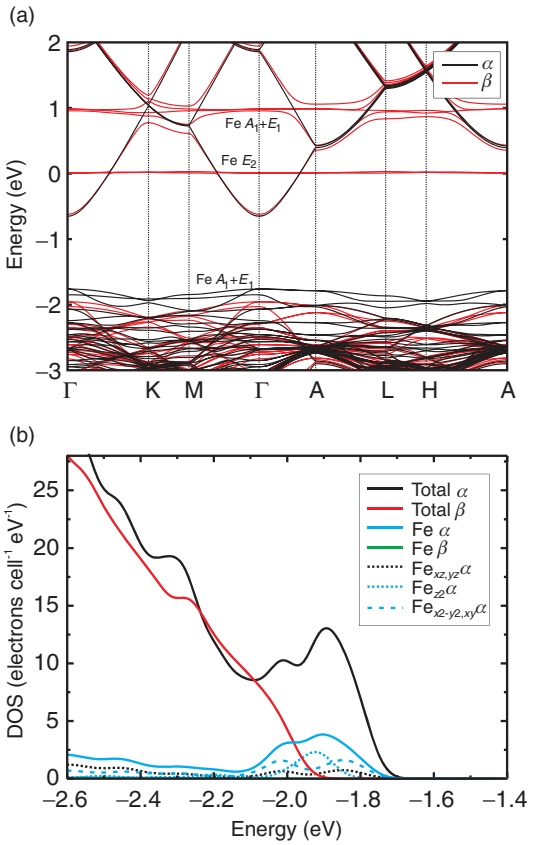

FIG. 16. (Color online) (a) Band structure of $Zn_{0.972}Fe_{0.028}O$ calculated with DFT along various directions of the ZnO Brillouin zone by using a $3 \times 3 \times 2$ supercell. Energy zero refers to the highest occupied level. (b) Valence-band DOS and selected projected DOS contributions of $Zn_{0.972}Fe_{0.028}O$ corresponding to the band structure shown in (a).

with O $2p_z$ states (in fact, the main contribution to the DOS at -1.45 eV comes from O $2p$ states). Following the discussion on $Zn_{1-x}Cu_xO$, the top of the alloy valence band should be the energy below which the total DOS is dominated by O $2p$ states (-1.35 eV). This energy corresponds to the top of the third α-spin band, with A_1 symmetry, that exhibits strong dispersion along the Γ-A direction and a strong anticrossing halfway in this direction at -1.45 eV, the energy around which the Ni $3d_{z^2}$ contribution has its maximum. Note that this assignment would result in a reversal of the wurtzite crystal field. Again, this anomalous result is a consequence of the ordered alloy symmetry. With this assignment, the band-gap coefficient for $Zn_{1-x}Ni_xO$ would be -41 meV/%Ni.

In the case of $Zn_{1-x}Fe_xO$ (Fig. 16), all β-spin Fe $3d$ states are inside the conduction band. Surprisingly, the Fe $3d$ E_2 state is inside the valence band (in spite of the fact that Fe is lighter than Co). The three α-spin bands at the top of the valence band have strong Fe $3d$ character, and, contrary to the case of $Zn_{1-x}Ni_xO$, the E_1 and A_1 Fe $3d$ states are close to each other and the A_1 band (Fe $3d_{z^2}$ contribution) does not cross the A_1 band along the Γ-A direction. The top of the alloy valence band should then be the E_1 band at -2.1 eV, energy at which the O $2p$ contribution is clearly dominant. With this assignment the band-gap coefficient would be 17 meV/%Fe.

VI. CONCLUSIONS

Thin films of wurtzite wide-gap DMS $Zn_{1-x}M_xO$ (M = Cr, Mn, Fe, Co, Ni, Cu) have been prepared by pulsed laser deposition and investigated by means of optical absorption at low temperature and photoelectron spectroscopy. It is found that the pure wurzite phase is kept for Co and Mn concentrations up to 25%, while in the case of Fe, Ni, and Cu, other phases are present for concentrations higher than 5, 2, and 1%, respectively. The band gap is found to increase at a rate of 9, 22, 23, and 4 meV/%M for $Zn_{1-x}M_xO$ with M = Cr, Mn, Co, and Fe, respectively, but to decrease at a rate of -14 and -9.8 meV/%M for M = Ni and Cu, respectively. The photoelectron spectroscopy study of the valence band of $Zn_{1-x}M_xO$ with M = Mn or Co led to the conclusion that the emergence of the TM-related photoemission peak is clearly correlated to a larger binding energy of the O $2p$ valence-band peaks. A simple model of p-d interaction is proposed in which the decrease of Zn $3d$ electron density below the valence band and the increase of M $3d$ electron density for M = Cr, Mn, Fe, and Co lead to higher binding energies of the valence band and, consequently, to a larger band gap. In contrast, for Ni and Cu, $3d$ electrons are more strongly bound than the O $2p$ ones and push them to lower binding energies, thus decreasing the band gap. This simple model was essentially confirmed by

first-principles DFT band structure calculations for $Zn_{1-x}M_xO$ alloys using a $3 \times 3 \times 2$ supercell corresponding to a substitution degree around 2.8%. The calculated band structures and DOS clearly showed that substitution with *M* having localized 3*d* DOS peaks above the O 2*p* peaks, the band gap of the alloy increases, while it decreases for substitution with *M* having 3*d* broad DOS peaks overlapping and strongly hybridizing with the O 2*p* bands. Analysis of these calculations also suggested that the *s*-*d* interaction plays a very important role for the more light *M* elements Cr and Mn.

ACKNOWLEDGMENTS

This work was supported by MINECO through Grants No. MAT2008-06873-C02-02, No. MAT2011-28868-C02-02, No. MAT2011-24757, No. FIS2009-12721-C04-03, and No. CSD2007-00041, the Generalitat Valenciana (Grants No. GV04A-123 and No. Prometeo-2009/074), and the Universitat de València for its V Segles and collaboration postgraduate research grants. Authors acknowledge technical and scientific assistance of Antares beamline staff of SOLEIL synchrotron.

[1] W. Pacuski, D. Ferrand, J. Cibert, C. Deparis, J. A. Gaj, P. Kossacki, and C. Morhain, Phys. Rev. B **73**, 035214 (2006).
[2] M. A. White, S. T. Ochsenbein, and D. R. Gamelin, Chem. Mater. **20**, 7107 (2008).
[3] J. A. Sans, A. Segura, J. F. Sánchez-Royo, Ch. Ferrer-Roca, and E. Guillotel, Phys. Status Solidi B **244**, 407 (2007).
[4] J. H. Kim, H. Kim, D. Kim, S. G. Yoon, and W. K. Choo, Solid State Commun. **131**, 677 (2004).
[5] K. J. Kim and Y. R. Park, Appl. Phys. Lett. **81**, 1420 (2002).
[6] S. Deka, R. Pasricha, and P. A. Joy, Phys. Rev. B **74**, 033201 (2006).
[7] K. Samanta, P. Bhattacharya, and R. S. Katiyara, Appl. Phys. Lett. **87**, 101903 (2005).
[8] L. Wei, Z. Li, and W. F. Zhang, Appl. Surf. Sci. **255**, 4992 (2009).
[9] T. Fukumura, Zhengwu Jin, A. Ohtomo, H. Koinuma, and M. Kawasaki, Appl. Phys. Lett. **75**, 3366 (1999).
[10] D. Y. Lin, H. J. Lin, J. S. Wu, W. C. Chou, C. S. Yang, and J. S. Wang, J. Appl. Phys. **105**, 053506 (2009).
[11] C. A. Johnson, K. R. Kittilstved, T. C. Kaspar, T. C. Droubay, S. A. Chambers, G. Mackay Salley, and D. R. Gamelin, Phys. Rev. B **82**, 115202 (2010).
[12] L. Xu and X. Li, J. Cryst. Growth **312**, 851 (2010).
[13] B. Marí, A. Elmanouni, L. Damonte, and M. Mollar, Phys. Status Solidi A **207**, 1623 (2010).
[14] C. Wang, Z. Chen, Y. He, L. Li, and D. Zhang, Appl. Surf. Sci. **255**, 6881 (2009).
[15] K. J. Kim and Y. R. Park, J. Appl. Phys. **96**, 4150 (2004).
[16] S. Yılmaz, M. Parlak, S. Özcan, M. Altunbas, E. McGlynn, and E. Bacaksız, Appl. Surf. Sci. **257**, 9293 (2011).
[17] Y. Liu, Y. Yang, J. Yang, Q. Guan, H. Liu, L. Yang, Y. Zhang, Y. Wang, M. Wei, X. Liu, L. Fei, and X. Cheng, J. Solid State Chem. **184**, 1273 (2011).
[18] W. Yu, L. H. Yang, X. Y. Teng, J. C. Zhang, Z. C. Zhang, L. Zhang, and G. S. Fu, J. Appl. Phys. **103**, 093901 (2008).
[19] D. Chakraborti, J. Narayan, and J. T. Prater, Appl. Phys. Lett. **90**, 062504 (2007).
[20] B. Hu, M. Adachi, K. Yamamoto, A. Nakamura, and J. Temmyo, Phys. Status Solidi C **7**, 1571 (2010).
[21] T. Dietl, H. Ohno, F. Matsukura, J. Cibert, and D. Ferrand, Science. **287**, 1019 (2000).
[22] M. Venkatesan, C. B. Fitzgerald, J. G. Lunney, and J. M. D. Coey, Phys. Rev. Lett. **93**, 177206 (2004).
[23] J. M. D. Coey, M. Venkatesan, and C. B. Fitzgerald, Nat. Mater. **4**, 173 (2005).
[24] S. H. Wei and A. Zunger, Phys. Rev. B **37**, 8958 (1988).
[25] S. H. Wei and A. Zunger, Phys. Rev. B **60**, 5404 (1999).
[26] J. A. Sans, A. Segura, M. Mollar, and B. Marí, Thin Solid Films **453-454**, 251 (2004).
[27] P. Hohenberg and W. Kohn, Phys. Rev. **136**, 864 (1964); W. Kohn and L. J. Sham, *ibid*. **140**, 1133 (1965).
[28] J. M. Soler, E. Artacho, J. D. Gale, A. García, J. Junquera, P. Ordejón and D. Sánchez-Portal, J. Phys.: Condens. Matter **14**, 2745 (2002).
[29] For more information on the SIESTA code visit: http://www.uam.es/siesta/
[30] For a review on applications of the SIESTA approach to materials science, see: D. Sánchez-Portal, P. Ordejón, and E. Canadell, Struct. Bonding (Berlin) **113**, 103 (2004).
[31] J. P. Perdew, K. Burke, and M. Ernzerhof, Phys. Rev. Lett. **77**, 3865 (1996).
[32] N. Trouiller and J. L. Martins, Phys. Rev. B **43**, 1993 (1991).
[33] L. Kleinman and D. M. Bylander, Phys. Rev. Lett. **48**, 1425 (1982).
[34] S. G. Louie, S. Froyen, and M. L. Cohen, Phys. Rev. B **26**, 1738 (1982).
[35] E. Artacho, D. Sánchez-Portal, P. Ordejón, A. García, and J. M. Soler, Phys. Status Solidi B **215**, 809 (1999).
[36] N. A. Spaldin, Phys. Rev. B **69**, 125201 (2004).
[37] E. Anglada, J. M. Soler, J. Junquera, and E. Artacho, Phys. Rev. B **66**, 205101 (2002).
[38] B. Meyer, H. Rabaa, and D. Marx, Phys. Chem. Chem. Phys. **8**, 1513 (2006).
[39] E. H. Kisi and M. M. Elcombe, Acta Crystallogr. Sec. C **45**, 1867 (1989).
[40] H. J. Monkhorst and J. D. Pack, Phys. Rev. B **13**, 5188 (1976).
[41] G. Martínez-Criado, A. Segura, J. A. Sans, A. Homs, J. Pellicer-Porres, and J. Susini, Appl. Phys. Lett. **89**, 061906 (2006).
[42] J. A. Sans, J. F. Sánchez-Royo, J. Pellicer-Porres, A. Segura, E. Guillotel, G. Martinez-Criado, J. Susini, A. Muñoz-Páez, and V. López-Flores, Superlattices Microstruct. **42**, 226 (2007).
[43] J. Pellicer-Porres, A. Segura, J. Sánchez-Royo, J. A. Sans, J. P. Itié, A. M. Flank, P. Lagarde, and A. Polian, Appl. Phys. Lett. **89**, 231904 (2006).
[44] S. Gilliland, A. Segura, J. F. Sánchez-Royo, L. M. García, F. Bartolomé, J. A. Sans, G. Martínez-Criado, and F. Jimenez-Villacorta, J. Appl. Phys. **108**, 073922 (2010).
[45] T. Makino, C. H. Chia, N. T. Tuan, Y. Segawa, M. Kawasaki, A. Ohtomo, K. Tamura, and H. Koinuma, Appl. Phys. Lett. **76**, 3549 (2000).
[46] S. G. Gilliland, J. A. Sans, J. F. Sánchez-Royo, G. Almonacid, and A. Segura, Appl. Phys. Lett. **96**, 241902 (2010).
[47] R. J. Elliott, Phys. Rev. **108**, 1384 (1957).
[48] Y. Toyozawa, Prog. Theor. Phys. **20**, 53 (1958).
[49] A. Ohtomo, M. Kawasaki, T. Koida, K. Masubuchi, H. Koinuma, Y. Sakurai, Y. Yoshida, T. Yasuda, and Y. Segawa, Appl. Phys. Lett. **72**, 2466 (1998).

[50]H. S. Kang, S. H. Lim, J. W. Kim, H. W. Chang, G. H. Kim, J.-H. Kim, S. Y. Lee, Y. Li, J.-S. Lee, J. K. Lee, M. A. Nastasi, S. A. Crooker, and Q. X. Jia, J. Cryst. Growth **287**, 70 (2006).
[51]J. Zúñiga-Pérez, V. Muñoz-Sanjosé, M. Lorenz, G. Benndorf, S. Heitsch, D. Spemann, and M. Grundmann, J. Appl. Phys. **99**, 023514 (2006).
[52]J. A. Sans, J. F. Sánchez-Royo, A. Segura, G. Tobias, and E. Canadell, Phys. Rev. B **79**, 195105 (2009).
[53]M. Kobayashi, Y. Ishida, J. I. Hwang, T. Mizokawa, A. Fujimori, K. Mamiya, J. Okamoto, Y. Takeda, T. Okane, Y. Saitoh, Y. Muramatsu, A. Tanaka, H. Saeki, H. Tabata, and T. Kawai, Phys. Rev. B **72**, 201201(R) (2005).
[54]S. C. Wi, J.-S. Kang, J. H. Kim, S.-B. Cho, B. J. Kim, S. Yoon, B. J. Suh, S. W. Han, K. H. Kim, K. J. Kim, B. S. Kim, H. J. Song, H. J. Shin, J. H. Shim, and B. I. Min, Appl. Phys. Lett. **84**, 4233 (2004).
[55]D. Iusan, R. Knut, B. Sanyal, O. Karis, O. Eriksson, V. A. Coleman, G. Westin, J. M. Wikberg, and P. Svedlindh, Phys. Rev. B **78**, 085319 (2008).
[56]S. Wei and A. Zunger, Appl. Phys. Lett. **72**, 2011 (1998).
[57]T. Makino, C. H. Chia, N. T. Tuan, H. D. Sun, Y. Segawa, M. Kawasaki, A. Ohtomo, K. Tamura, and H. Koinuma, Appl. Phys. Lett. **77**, 975 (2000).
[58]K. Zitouni, A. Kadri, P. Lefebvre, and B. Gil, Superlattices Microstruct. **39**, 91 (2006).
[59]G. Coli and K. K. Bajaj, Appl. Phys. Lett. **78**, 2861 (2001).
[60]B. Laumer, T. A. Wassner, F. Schuster, M. Stutzmann, J. Schörmann, M. Rohnke, A. Chernikov, V. Bornwasser, M. Koch, S. Chatterjee, and M. Eickhoff, J. Appl. Phys. **110**, 093513 (2011).
[61]W. R .L. Lambrecht, A. V. Rodina, S. Limpijumnong, B. Segall, and B. K. Meyer, Phys. Rev. B **65**, 075207 (2002).
[62]K. Sato and H. Katayama-Yoshida, Jpn. J. Appl. Phys. **39**, L334 (2000).
[63]K. Sato and H. Katayama-Yoshida, Physica B **308**, 904 (2001).
[64]K. Sato and H. Katayama-Yoshida, Phys. Status Solidi B **229**, 673 (2002).
[65]C.-H. Chien, S. H. Chiou, G. Y. Guo, and Y. D. Yao, J. Magn. Magn. Mater. **282**, 275 (2004).
[66]X. Feng, J. Phys.: Condens. Matter. **16**, 4251 (2004).
[67]S. Y. Yun, G.-B. Cha, Y. Kwoon, S. Cho, and S. C. Hong, J. Magn. Magn. Mater. **272-276**, e1563 (2004).
[68]Y. Imai and A. Watanabe, J. Mater. Sci. **15**, 743 (2004).
[69]P. Gopal and N. A. Spaldin, Phys. Rev. B **74**, 094418 (2006).
[70]P. Palacios, I. Aguilera, and P. Whanon, Thin Solid Films **518**, 4568 (2010).
[71]D. Q. Thomas, J. Phys. Chem. Solids **15**, 86 (1960).